Biochimica et Biophysica Acta 1840 (2014) 322–331

Contents lists available at ScienceDirect

Biochimica et Biophysica Acta

journal homepage: www.elsevier.com/locate/bbagen

Nonsteroidal anti-inflammatory drug sulindac sulfide suppresses structural protein Nesprin-2 expression in colorectal cancer cells☆

Jason L. Liggett [a,1], Chang Kyoung Choi [a,e,1], Robert L. Donnell [a], Kenneth D. Kihm [b], Jong-Sik Kim [c], Kyung-Won Min [a], Angelika Anna Noegel [d], Seung Joon Baek [a,*]

[a] Department of Biomedical and Diagnostic Sciences, University of Tennessee, Knoxville, TN 37996, USA
[b] Department of Mechanical, Aerospace, and Biomedical Engineering, University of Tennessee, Knoxville, TN 37996, USA
[c] Department of Biology, Andong National University, Andong, Republic of Korea
[d] Institute for Biochemistry, University of Cologne, 50931 Cologne, Germany
[e] Department of Mechanical Engineering–Engineering Mechanics, Michigan Technological University, Houghton, MI 49931, USA

ARTICLE INFO

Article history:
Received 18 March 2013
Received in revised form 22 August 2013
Accepted 20 September 2013
Available online 27 September 2013

Keywords:
Nesprin-2
NUANCE
NSAID
Colon cancer
Micro-impedance
NAG-1

ABSTRACT

Background: Nonsteroidal anti-inflammatory drugs (NSAIDs) are well known for treating inflammatory disease and have been reported to have anti-tumorigenic effects. Their mechanisms are not fully understood, but both cyclooxygenase (COX) dependent and independent pathways are involved. Our goal was to shed further light on COX-independent activity.
Methods: Human colorectal cancer cells were observed under differential interference contrast microscopy (DICM), fluorescent microscopy, and micro-impedance measurement. Microarray analysis was performed using HCT-116 cells treated with sulindac sulfide (SS). PCR and Western blots were performed to confirm the microarray data and immunohistochemistry was performed to screen for Nesprin-2 expression. Micro-impedance was repeating including Nesprin-2 knock-down by siRNA.
Results: HCT-116 cells treated with SS showed dramatic morphological changes under DICM and fluorescent microscopy, as well as weakened cellular adhesion as measured by micro-impedance. Nesprin-2 was selected from two independent microarrays, based on its novelty in relation to cancer and its role in cell organization. SS diminished Nesprin-2 mRNA expression as assessed by reverse transcriptase and real time PCR. Various other NSAIDs were also tested and demonstrated that inhibition of Nesprin-2 mRNA was not unique to SS. Additionally, immunohistochemistry showed higher levels of Nesprin-2 in many tumors in comparison with normal tissues. Further micro-impedance experiments on cells with reduced Nesprin-2 expression showed a proportional loss of cellular adhesion.
Conclusions: Nesprin-2 is down-regulated by NSAIDs and highly expressed in many cancers.
General significance: Our data suggest that Nesprin-2 may be a potential novel oncogene in human cancer cells and NSAIDs could decrease its expression.

1. Introduction

Nonsteroidal anti-inflammatory drugs (NSAIDs) are widely used in the treatment of inflammatory disease through inhibition of prostaglandin production by cyclooxygenase-2 (COX-2). Interestingly, COX-2 expression is up-regulated in human colorectal tumors and regulates tumor growth in animal models [1–3]. NSAIDs have been shown to inhibit incidence and mortality of colorectal cancer in a broad range of studies [4,5]. Although the chemopreventive and anti-tumorigenic activity of NSAIDs in cancer is well established, the molecular mechanisms responsible have not been completely elucidated.

The NSAID sulindac sulfide (SS) inhibits growth of tumors in azoxymethane-induced rat colon models [6], suppresses intestinal polyp formation in APC^{Min+} mice [7,8], down-regulates β-catenin protein apoptosis [9], and induces apoptosis under a number of experimental conditions [10–12]. SS has been shown to change colorectal cancer cell morphology [13], alter cytoskeletal organization, and cause loss of actin stress fibers [14,15]. This is probably due to a dose-dependent reduction of tyrosine phosphorylation of focal adhesion kinase [15]. It has also been demonstrated that SS reduces cell migration and invasion in mouse models and human colorectal cell lines [16,17].

Abbreviations: NSAID, nonsteroidal anti-inflammatory drug; SS, sulindac sulfide; NAG-1, NSAID activated gene 1

☆ Grant supports: This work was supported by the American Cancer Society (CNE-111611), the National Institutes of Health (R01CA108975), and the Center of Excellence in Livestock Diseases and Human Health, University of Tennessee, to S.J.B.

* Corresponding author at: Department of Biomedical and Diagnostic Sciences, College of Veterinary Medicine, The University of Tennessee, 2407 River Drive, Rm A228, Knoxville, TN 37996, USA. Tel.: +1 865 974 8216; fax: +1 865 974 5616.
E-mail address: sbaek2@utk.edu (S.J. Baek).

[1] Authors contributed equally to the paper.

0304-4165/$ – see front matter © 2013 Elsevier B.V. All rights reserved.
http://dx.doi.org/10.1016/j.bbagen.2013.09.032

We speculated that SS alters gene expression related to cell organization, and subsequently we found the structural gene Nesprin-2 (NUANCE/Syne-2) was down-regulated in two independent microarrays using two different doses of SS-treated human colorectal cancer cells. Nesprin-2 is a giant protein with an α-actinin-like actin binding domain [18]. To date, together with the closely related Enaptin/Nesprin-1, Nesprin-2 is the largest of the α-actinin superfamily, and it encodes a 796 kDa protein containing an N-terminal actin-binding domain, central coiled-coil rod domain, and a C-terminal transmembrane domain [18,19]. Nesprin-2 also has many truncated alternate splicing forms [20,21]. The majority of Nesprin-2 is localized to the nuclear envelope, while a very small fraction can be found in the cytoplasm; the tissue distribution of Nesprin-2 mRNA is fairly ubiquitous with most tissues, showing at least trace amounts [18]. Recently Nesprin-2 has been shown to affect nuclear size and to be involved in regulating genes during wound healing [22,23]. This colossal protein contains multiple binding sites and serves as a framework for protein complexes on the nuclear envelope [24,25].

In this study, we found that human colorectal cancer HCT-116 cells dramatically changed their morphology and cell adhesion by SS, as assessed using biological, chemical, optical, and electrical methods. Subsequently, Nesprin-2 was identified and confirmed as being down-regulated by SS. Finally, we showed that Nesprin-2 is more highly expressed in tumor tissues, compared to normal tissues, suggesting that Nesprin-2 may be a novel oncogene.

2. Materials and methods

2.1. Reagents

The NSAIDs used in this study were purchased as follows: SS, tolfenamic acid, and SC-560 from Cayman Chemical Company (Ann Arbor, Michigan); diclofenac from Sigma-Aldrich (St. Louis, MO); and 5,5-dimethyl-3-(3-fluorophenyl)-4-(4-ethylsulfonyl)phenyl-2(5*H*)-furanone (DFU) was as a gift from Merck (Rahway, NJ).

All other chemicals were purchased from Fisher Scientific, unless otherwise specified.

2.2. Cell culture

All cells were purchased from ATCC and grown at 37 °C with 5% CO_2. HCT-116 and HT-29 cells were cultured with McCoy's 5A modified media. HCT-116 cells were kept to fewer than 20 passages to maintain the expected cellular mutations. SW480 cells were cultured with RPMI-1640. All culture media was supplemented with 10% fetal bovine serum, 100 μg/ml streptomycin, and 100 UI penicillin. Serum free media was used for all SS and vehicle treatments unless stated otherwise.

2.3. Microscopic measurement

Three microscopic techniques were employed, differential interference contrast microscopy (DICM) and epi-fluorescence microscopy (EFM) for imaging the whole cell including dorsal surface, as well as interference reflection contrast microscopy (IRCM) for imaging the ventral surface of cells. The microscopic imaging system consisted of an Olympus IX-71 inverted microscope, a plan apochromat 100× oil immersion objective with adjustable numerical aperture, 14-bit electron multiplier charge coupled device from Hamamatsu, and an incubation chamber that kept the temperature (37 °C), humidity, and CO_2 (5%) levels constant. In order to examine the entire cellular morphology response to SS using DICM and EFM, HCT-116 cells were plated at a concentration of 1×10^5 cells/ml. After 24 h, cells were stained with LavaCell™ solution (Active Motif, Carlsbad, CA) to a concentration of 0.6 μM for 6 h. Next, the media was changed to serum-free media containing 30 μM SS, and the cells were monitored microscopically for the next 6 h. IRCM was used to examine the bottom morphology changes of HCT-116 cells exposed to 10 μM and 30 μM SS.

2.4. Electrical impedance measurements

A data acquisition and analysis system was implemented using LabVIEW (National Instruments, Austin, TX). Preliminary naked scans were performed to optimize sensitivity and to check for any electrode debris or defects. The electrodes were then inoculated with 400 μl media containing HCT-116 cells at a concentration of 2.4×10^4 cells/ml under a range of SS concentrations. During the cellular micro-impedance scans, data was acquired at a rate of 32 Hz for 16 s using a 30 ms filter time constant and 12 dB/decade roll off for approximately 96 h. Averages and standard deviation estimates were obtained from 512 sampled data points over the 16 s time intervals. During the experiments, cell-inoculated electrodes were kept in a cell culture incubator.

2.5. Microarrays

Two independent microarray experiments were performed: Human Array-Illumina HEEBO oligo microarray and Agilent oligo microarray. The 48.5 K Human Array-Illumina HEEBO oligo microarray was purchased from Microarrays Inc. (Nashville, TN). RNA was isolated from DMSO or 5 μM treated HCT-116 cells after 24 h. One microgram of total RNA was used to synthesize cDNA. The arrays were hybridized at 42 °C for 12–16 h in a humidified hybridization chamber (GenomicTree, Korea). After washing, microarrays were immediately dried using the microarray centrifuge (GenomicTree, Korea). The hybridization images were analyzed by GenePix Pro 6.0 (Axon Instruments, Sunnyvale, CA). Another microarray analysis was conducted using Agilent human oligo 1A arrays (Agilent Technologies, Palo Alto, CA). HCT-116 cells were treated with DMSO or 10 μM SS for 24 h. Total RNA was amplified using the Agilent Low RNA Input Fluorescent Linear Amplification Kit protocol. Starting with 500 ng of total RNA, Cy3- or Cy5-labeled cRNA was produced according to manufacturer's protocol. For each two color comparison, 750 ng of each Cy3 and Cy5 labeled cRNAs was mixed and fragmented using the Agilent *In Situ* Hybridization Kit protocol. Hybridizations were performed using the Agilent 60-mer oligo microarray processing protocol. Data was obtained using Agilent Feature Extraction software v7.5. Intensity plots were generated for each ratio experiment, and genes were considered "signature genes" if the P value was less than 0.001. Functional annotation of genes was performed according to the Gene Ontology Consortium (http://www.geneontology.org/index.shtml) by GeneSpring v7.3.

2.6. Reverse transcriptase PCR and real time PCR

RNA was isolated from cell cultures using Qiagen's RNeasy Mini Kit following the manufacturer's protocol. One microgram of RNA was used to generate cDNA using Bio-Rad's iScript™ cDNA Synthesis Kit following the manufacturer's protocol. PCR was performed with the following primers: Nesprin-2 Giant forward 5′-CAGTCCTTACAACTCCT GGACAC-3′, Nesprin-2 Giant reverse 5′-GACTGATTCTCCTACCCACAG ACTC-3′; Nesprin-2 all isoforms forward 5′-TCACAGAGCAGCAGTCA GGT-3′, Nesprin-2 all isoforms reverse 5′-GCTCACGTTGACAGAGACCA-3′; Nesprin-2 α_1 forward 5′-GCAGAAGCCTATGA GTTG-3′, Nesprin-2 α_1 & α_2 reverse 5′-TGTAGTGATGCTCGGGACAG-3′; Nesprin-2 α_2 forward 5′-CATCCCACAGCAATCATG-3′; Nesprin-1 forward 5′-GGCTGAAA ATCGAAGAGACG-3′, Nesprin-1 reverse 5′-CATCTC TGTGAGCCAGAC CA-3′; GAPDH forward 5′-GGGCTGCTTTTAACTCTGGT-3′, GAPDH reverse 5′-TGGCAGGTTTTTCTAGACGG-3′; IDH2 forward 5′-GACGGAGA TGTGCAGTCAGA-3′, IDH2 reverse 5′-GTCCGTGGTGTTCAGGAAGT-3′; NAG-1 forward 5′-CTCCAGATTCCGAGAGTTGC-3′, and NAG-1 reverse 5′-AGAGATACGCAGGTGCAGGT-3′. Densitometric analysis of reverse transcriptase PCR was performed using Scion Image software

(Frederick, MD). Real time PCR was performed using Thermo Scientific's ABsolute qPCR SYBR Green Mix (Waltham, MA) on a Bio-Rad MyiQ iCycler thermal cycler using Bio-Rad iQ5 version 2.1 software following the manufacture's protocol (Hercules, CA). Measurements were standardized using GAPDH, and each set of three or more trials was averaged.

2.7. Immunohistochemistry

Immunostaining on a Biochain Tissue Array Human Tumor Tissue II (Lot# A711214) slide was performed using standard immunohistochemistry procedures (T8235713-2; Newark, CA). The slide was incubated overnight at 4 °C with undiluted mAB K20-478 hybridoma antibody against Nesprin-2 [18] and secondary antibody treatment was performed using biotinylated anti-mouse immunoglobulins from BioGenex (HK-335-9M; San Ramon, CA). Nesprin-2 protein was stained brown with Chromogen-DAB solution and cells were counterstained with Hematoxylin (Richard Allen Scientific, Kalamazoo, MI). Tissues were rated for stain intensity by microscopic examination of three observers. An Olympus BX41 microscope with an Olympus DP70 digital camera employing integrated software was used for image capture/scaling.

2.8. Transfection of Nesprin-2 siRNA

HCT-116 cells were transfected with siRNA using PepMute reagent for 24 h (SignaGen, Rockville, MD) following the manufacturer's protocol. The final concentration of siRNA was 10 nM for both the Control siRNA-A (sc-37007), and Syne-2 siRNA (sc-61630, Santa Cruz Biology, Inc., Santa Cruz, LA). After 24 h, the media was changed with fresh complete media and allowed to grow for 24 more hours. The cells were then suspended and diluted to 2.4×10^4 cells/ml with McCoy's 5A modified media. Cells were then treated with either DMSO or 30 μM SS. These cells were used for impedance experiments and harvested to isolate RNA for real time PCR.

The cells were suspended and diluted to 2.4×10^4 cells/ml with McCoy's 5A modified media. Cells were then treated with either DMSO or 30 μM SS. These cells were used for impedance experiments and harvested to isolate RNA for PCR.

2.9. RNA stability

HCT-116 cells were plated in 6 well plates (6×10^5 cells/ml) and grown until ~90% confluence. The cells were washed with PBS and pre-treated with 5 μM actinomycin D in serum free media for 1 h, and then the vehicle and 30 μM SS (final concentration) were added to the serum free media containing actinomycin D. RNA isolation, cDNA synthesis, and reverse transcriptase PCR were performed as previously described in Section 2.6.

2.10. Western blot

Cells lysates were isolated in RIPA buffer (50 mM Tris–HCl pH 7.4, 150 mM NaCl, 1 mM EDTA, 1% Triton X-100, 1% sodium deoxycholate, 0.1% SDS) supplemented with protease inhibitors (1 mM PMSF, 1 μg/ml aprotinin, 1 μg/ml leupeptin) and phosphatase inhibitors (10 mM NaF, 0.1 mM Na_3VO_4). Protein concentration was determined by BCA protein assay (Pierce, Rockford, IL). The proteins were separated on SDS-PAGE and transferred to nitrocellulose membranes (Osmonics, Minnetonka, MN). The membranes were incubated with anti-Nesprin-2 (sc-51220, Santa Cruz Biotechnology, Inc., Santa Cruz, CA) in 1% bovine serum albumin at 4 °C overnight. After three washes with Tris buffered saline containing 0.05% Tween 20, the blots were incubated with peroxidase-conjugated IgG for 1 h at room temperature and visualized using ECL (Amersham Biosciences, Piscataway, NJ) and a LAS-4000 mini (Fujifilm Life Sciences, Stamford, CT).

2.11. Statistics

Unless stated otherwise statistical significance was determined using single-tailed paired Student *t* tests. P-values are noted with asterisks as follows: *P < 0.05, **P < 0.01, and ***P < 0.001.

3. Results

3.1. Changes to cell adhesion and morphology during SS treatment in HCT-116 cells

Micro-impedance measurements were used to quantitatively examine relative changes in proliferation and morphology, due to the modulations in cell–cell adhesion, cell–substrate adhesion, and plasma membrane capacitance under different concentrations of SS. It is well known that NSAIDs alter cell morphology and adhesion in cell culture [15]. Resistance and reactance are both measured as functions of time and AC frequencies; Fig. 1A and B presents results only at representative frequencies of 5.62 kHz and 100 kHz, respectively. These changes are represented as the induction of apoptosis [26,27]. Higher concentrations of SS produced a reduction in the normalized impedance components, reflecting changes in cell–cell adhesion and cell–substrate adhesion (resistance, Fig. 1A), and the capacitance of the plasma membrane (reactance, Fig. 1B). The suppression of cell–cell adhesion and cell–substrate adhesion by SS appears to be a dose- and time-dependent manner. To examine cellular morphology HCT-116 cells were treated with SS in the presence of LavaCell staining solution, which stains only the cytoplasm and the nuclear membrane and is not cytotoxic under these conditions. As shown in Fig. 1C, SS changes cell morphology causing cellular rounding and nuclear condensation. Interestingly the apoptotic feature, “blebbing”, can be clearly seen under SS treatment (Fig. 1C, arrows). IRCM imaging shows dynamic gap morphology responses of live cells under SS treatment; dark areas indicate tight focal adhesion points between cell and substrate while lighter areas show increased gap between cell and substrate (Fig. 1D). Higher concentrations of SS showed a more dramatic increase in cellular gap from substrate and most bottom contacts including the close contacts as well as the remaining brighter areas noticeably diminished in response to the cellular shrinkage and retraction caused by SS, while some of the tightest focal contacts remain along the periphery of cells (Fig. 1D). Thus, SS induces loose adhesion between cells and substrate which results in cellular apoptosis.

3.2. Down-regulated cell organization and biogenesis genes

To elucidate molecular mechanisms by which SS affects cell morphology two independent microarray experiments were performed and compared. The genes of interest using SS-treated HCT-116 cells were chosen for function in “cellular organization and biogenesis” using the Gene Ontology Consortium. Surprisingly, only two genes, isocitrate dehydrogenase 2 (IDH2) and Nesprin-2, were commonly down-regulated and no genes were commonly up regulated between these two microarrays (Table 1). These genes represent potential targets of SS. IDH2 is a mitochondrial isozyme and Nesprin-2 is a large structural protein. Nesprin-2 was selected for further study based on its higher fold reduction compared to IDH2 and its unique role as a link between the actin cytoskeleton and the nuclear envelope as well as its novelty as a potential oncogene.

3.3. Microarray confirmation of genes down-regulated by sulindac sulfide

Down-regulation of Nesprin-2 and IDH2 mRNA by SS was confirmed by PCR in three replicates, standardized to GAPDH as a positive control (Fig. 2A). The fold reductions in these two genes correlate with the microarray data in that Nesprin-2 is more strongly down-regulated than IDH2 in both cases. We also examined NAG-1 (positive control) and

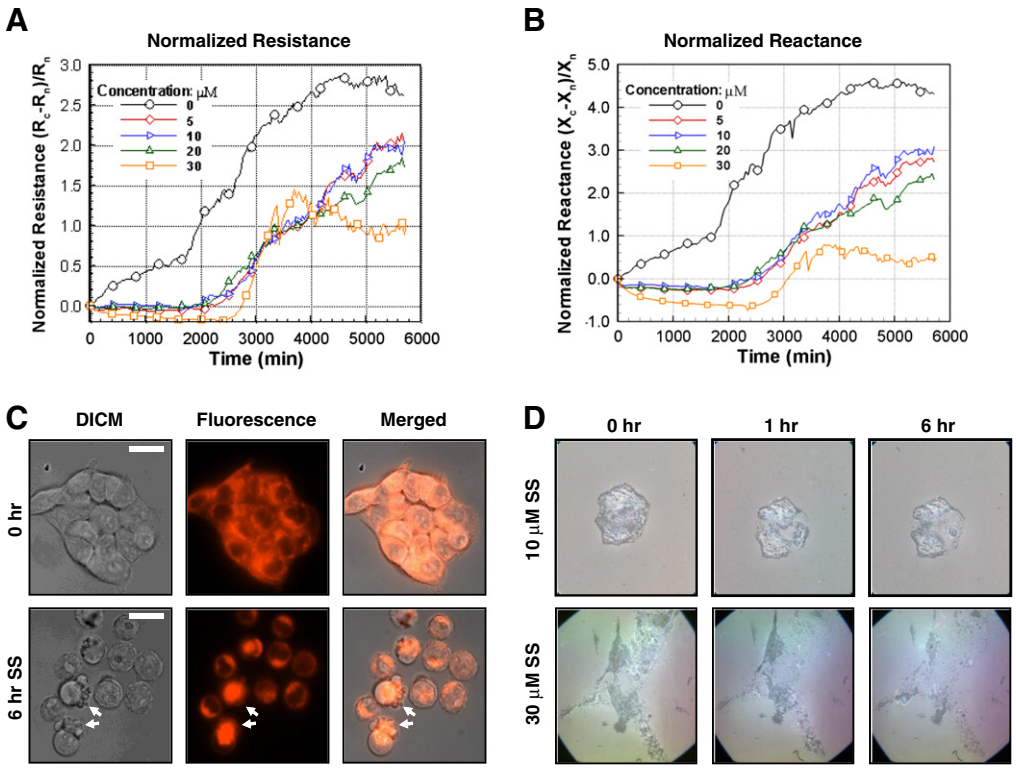

Fig. 1. HCT-116 cell adhesion and morphology during SS treatment. Biosensors were used to examine the dynamic attachment and spreading of colorectal cancer cells by monitoring micro-impedances. (A) The corresponding normalized resistance of HCT-116 cells. (B) The corresponding normalized reactance of HCT-116 measured for the same cells. The terms *R* and *X* represent the resistance and reactance, respectively, and the subscripts *c* and *n* indicate cell covered and naked scans, respectively. Symbols represent 20 data intervals. (C) Cellular morphology of HCT-116 cells was observed during 6 h, 30 μM SS treatment in a real time manner. Observations were made using DICM and EFM. LavaCell (0.6 μM) was used for staining the cytoplasm & membranes. The arrows indicate apoptotic blebbing. Scale bars represent 10 μm. (D) IRCM images to examine cellular gap morphology responses of HCT-116 cancer cells under SS treatment.

Nesprin-1 expression. NAG-1 has been known to be induced by SS [28] whereas Nesprin-1 is another form of Nesprin family proteins. Interestingly Nesprin-1 did not show any alterations in the presence of SS (Fig. 2A) indicating that NSAIDs affect Nesprin-2 in a specific manner. As shown in Fig. 2A, Nesprin-2 repression was significant at $P < 0.001$ and IDH2 was reduced at $P < 0.05$. Protein expression of truncated Nesprin-2 forms was checked by Western blot to verify that the mRNA reduction actually translates into a loss of protein expression in cells after an initial screen of many cell lines for detectable levels of Nesprin-2 isotypes (Fig. 2B and data not shown). Both HCT-116 and HepG2 cells showed a reduction by SS of a specific Nesprin-2 band (Fig. 2B). There are two Nesprin-2 alternate splicing variants that are close to the observed Nesprin-2 protein size, Nesprin-2 α_1 and Nesprin-2 α_2. To help differentiate between these two variants, specific forward PCR primers were designed utilizing differences in their 5′ untranslated regions (diagram showing primer locations in Fig. 2C). Reverse transcriptase PCR was performed on HCT-116 cells treated with vehicle or 30 μM SS for 24 h and showed down-regulation in all sets (Fig. 2C). The results indicate that there is very little Nesprin-2 α_1 expression compared to Nesprin-2 α_2 (Fig. 2B). This data taken into account with the size of the Nesprin-2 Western blot indicate that this band is the 48 kDa Nesprin-2 α_2 isoform.

3.4. Nesprin-2 was down-regulated by several NSAIDs in a time- and dose-dependent manner through RNA stability

Nesprin-2 has previously been reported in the leading edge of migrating cells in wound-healing assays [18]. Due to this and its structural role, Nesprin-2 is an excellent candidate for investigation of the effects of SS on cell morphology and adhesion. Nesprin-2 mRNA was suppressed in a time-dependent manner with significant reductions beginning at 6 h of treatment, $P < 0.01$ (Fig. 3A). Nesprin-2 down-regulation by SS was also dose-dependent, starting with 1 μM up to 30 μM (Fig. 3B). Next, a range of other NSAIDs was tested to see if Nesprin-2 reduction is unique to SS or common among NSAIDs. A wide range of NSAIDs were used including conventional NSAIDs, which inhibit both COX-1 and COX-2 (SS, tolfenamic acid, and diclofenac) as well as the COX-1 specific inhibitor SC-560 and the COX-2 specific inhibitor DFU. All NSAIDs significantly reduced Nesprin-2 mRNA expression at $P < 0.05$, with the most dramatic

Table 1
Down-regulated genes by sulindac sulfide in cell organization and biogenesis. Two independent oligo microarray experiments were performed on HCT-116 cells, treated by either 5 μM or 10 μM of SS. Functional annotation of genes was performed according to Gene Ontology Consortium by GeneSpring 7.3. The two microarrays were compared for commonly up- and down-regulated genes in the categories of cell organization and biogenesis. The only two common genes with a cut off of a 1.5 fold change were IDH2, a mitochondrial isozyme, and Nesprin-2, a large structural protein.

Gene name	Other names	GenBank acc. no.	Gene description	5 μM SS	10 μM
IDH2	IDH, IDP, IDHM, ICD-M	NM_002168	Isocitrate dehydrogenase 2 (NADP+), mitochondria	−1.37	−1.52
Nesprin-2	NUA, SYNE-2, NUANCE	NM_015180	Nucleus and actin connecting element	−1.99	−1.75

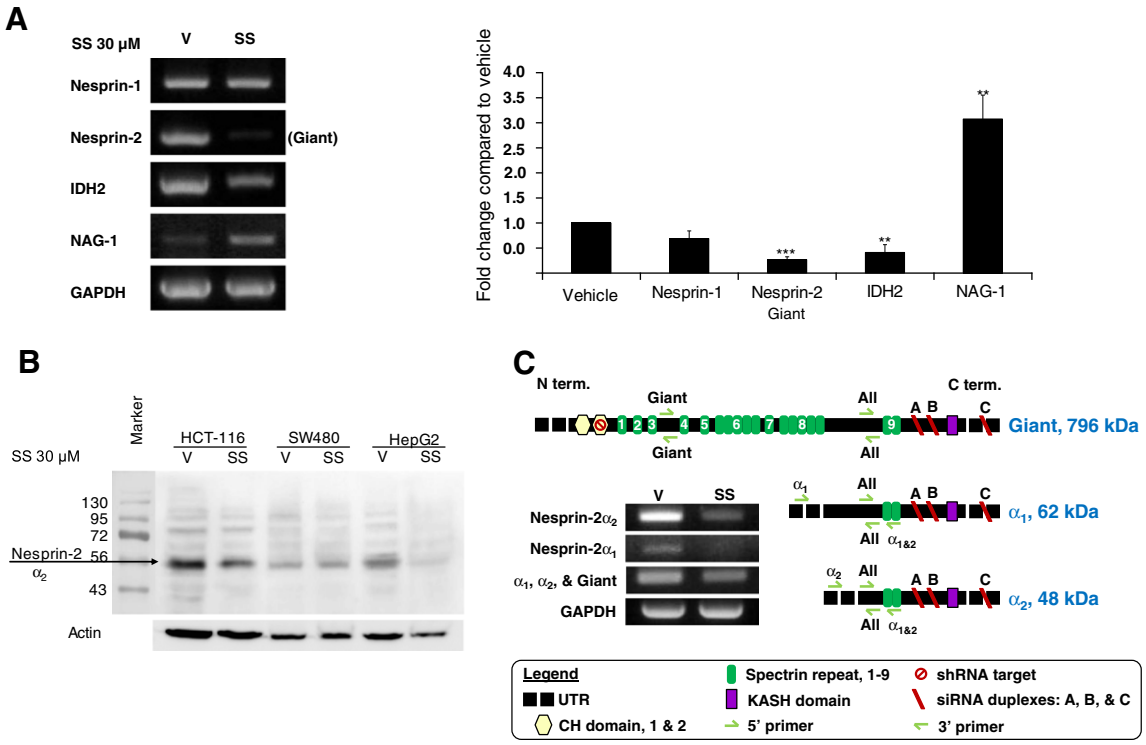

Fig. 2. Microarray conformation of genes down-regulated by SS. (A) HCT-116 cells were treated with 30 μM SS for 24 h, and three replicates of reverse transcriptase PCR were performed. Representative gel electrophoresis images are shown with NAG-1 as a positive control for SS treatment and GAPDH as a loading control. Averages of densitometer analysis of mRNA expression levels from the three replicates were normalized to GAPDH and compared to the vehicle. The data represent mean ± S.E. P-values of **, $P < 0.01$, and ***, $P < 0.001$. (B) Western blot analysis of cells treated with vehicle or 30 μM SS for 24 h using anti-Nesprin-2 targeting the C-terminal region. The arrow indicates the Nesprin-2 α_2. (C) Schematic diagram showing Nesprin-2 isoforms: Giant, α_1, and α_2. Locations of PCR primers, siRNA targets, and shRNA targets are shown. Reverse-transcriptase PCR data shows the effect of 30 μM SS for 24 h using primers specific for Nesprin-2 α_1, specific for Nesprin-2 α_2, and primers which amplify most isoforms of Nesprin-2 including: Giant, α_1, and α_2. Nesprin-2 Giant specific primers are shown in (A).

repression by SS (Fig. 3C). Interestingly, SS repression of Nesprin-2 is not limited to HCT-116 cells; however, this does not occur in all colorectal cancer cell lines tested. Sulindac sulfide treatment for 24 h significantly reduced Nesprin-2 in HT-29 cells; however, SW480 cells showed a reduction in Nesprin-2 with no statistical significance (Fig. 3D). HCT-116 cells and SW480 cells are both COX-1 and COX-2 negative, while HT-29 cells are wild type for COX-1 and COX-2; this suggests that SS decreases Nesprin-2 mRNA independently of cyclooxygenase expression. To elucidate a molecular mechanism by which SS suppressed Nesprin-2 expression, we examined RNA stability of Nesprin-2 in the presence of SS. HCT-116 cells were pre-treated with actinomycin D to inhibit transcription and a SS time course was carried out; Nesprin-2 mRNA was degraded slightly faster under SS treatment with 50% reduction of mRNA at 11.2 h, compared to vehicle's 16.8 h, based on the best fit linear regression trend lines (Fig. 3E). This suggests that SS facilitates Nesprin-2 RNA degradation, thereby reducing Nesprin-2 RNA transcripts.

3.5. Protein expression of Nesprin-2 in normal and tumor tissues

A tissue array slide containing a range of normal and neoplastic tissues was used to study Nesprin-2 protein expression on the microscopic level. The majority of the normal and neoplastic tissues in the array did not have detectable levels of positive staining, although the antibody detects all isotypes. Increased immunohistochemical staining of Nesprin-2 protein was observed in the neoplastic epithelial cells in tissues of the breast, duodenum, rectum, and thyroid, compared to normal tissue (Fig. 4, Supplemental Table 1). Focal to diffuse, mild to moderate positive staining was present within the cytoplasm of neoplastic cells. Discernible cytoplasmic staining of normal cells was limited to rare foci of crypt cells in the rectum. Although Nesprin-2 has been primarily detected in the nuclear membrane [18], our data suggest Nesprin-2 expression mostly in the cytoplasm. This cytoplasmic localization in multiple neoplastic epithelial cells as well as the proliferative crypt cells of the rectum supports Nesprin-2's potential role as an oncogene.

3.6. siRNA knock-down of Nesprin-2 expression's effect on cell impedance

The micro-impedance experiment was performed on HCT-116 cells either transfected with siRNA against Nesprin-2 or non-targeting control siRNA, then treated with vehicle or SS. The Nesprin-2 siRNA targets regions near the Nesprin-2 KASH domain which are present on Nesprin-2 Giant, α_1, and α_2 isoforms (Fig. 2C). In the case of the SS-treated cells, initial adhesion was similar at first for both Nesprin-2 knock-down and non-targeting control cells. After approximately a day and a half the Nesprin-2 knock-down cells showed reduced adhesion compared to the non-targeting control cells (Fig. 5B and C). The average reduction in Nesprin-2 mRNA when adjusted by GAPDH was a knock-down of 53% (Fig. 5A). Cell–cell adhesion and cell–substrate adhesion seen in the normalized resistance and plasma membrane capacitance in the normalized reactance of the Nesprin-2 knock-down cells, as compared with the control siRNA transfected cells treated with vehicle showed a reduction ranging from 50% after two days when the cells were most actively growing to 20% at completion of the three and a half day experiment (Fig. 5B and C). This suggests that reduction in Nesprin-2 by SS treatment could be contributing to the loss of adhesion in colorectal cancer cells. The Nesprin-2 shRNA was utilized to block Nesprin-2 expression. Although shRNA transfection marginally inhibits Nesprin-2 expression, similar results of impedance were observed (Supplementary data).

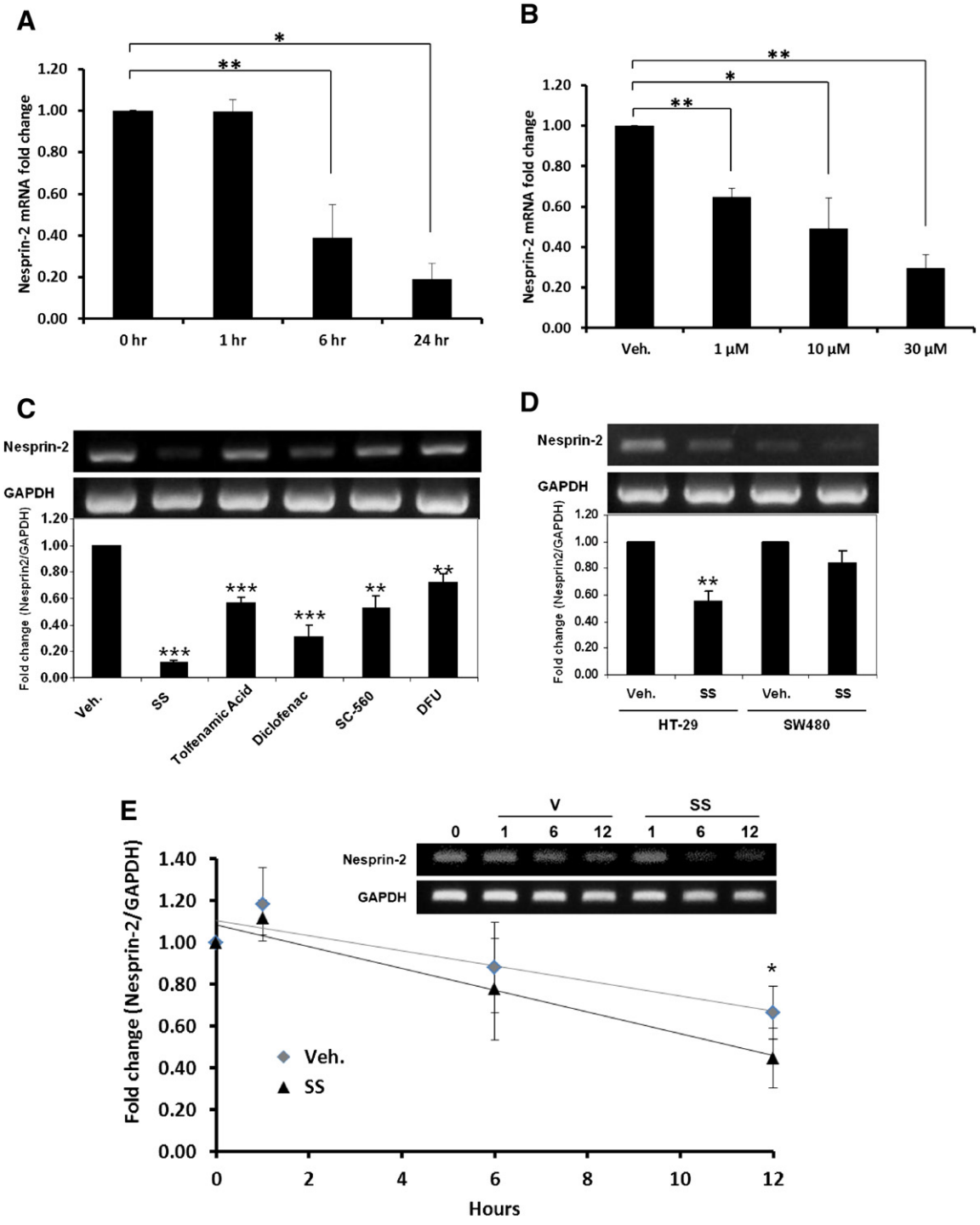

Fig. 3. Nesprin-2 mRNA expression in a time- and dose-dependent manner. (A) Nesprin-2 down-regulation by SS was shown by real time PCR to be time-dependent over a 24 h time course for HCT-116 cells treated with 30 μM SS. (B) HCT-116 cells also showed a dose-dependent response by real time PCR to SS over a 24 h treatment. (C) A variety of NSAIDs (SS 30 μM, tolfenamic acid 20 μM, diclofenac 100 μM, SC-560 25 μM, and DFU 100 μM) were tested on HCT-116 cells for 24 h (reverse transcriptase PCR). (D) Other colorectal cancer cell lines, HT-29 and SW480, were tested for Nesprin-2 suppression by reverse transcriptase PCR with SS after 24 h treatments. (E) Reverse transcriptase PCR on HCT-116 cells pre-treated with 5 μM actinomycin D for 1 h prior to a SS time course was performed and lines indicate a linear regression trend. Representative reverse transcriptase-PCR data and the densitometry results (bottom) as well as real time PCR data are shown from at least three independent experiments normalized to GAPDH and compared to 0 h (A & E) or vehicle (B, C, & D). The data represent mean ± S.E. *P < 0.05, **P < 0.01, and ***P < 0.001.

4. Discussion

There are several well-known methods to examine cell proliferation and morphological changes under specific treatments including fluorescence microscopy, flow cytometry, and biochemical assays. While these methods are stationary and need fluorescent or radioactive probes, micro-impedance measurement is a bio-analytical technique that is capable of non-invasively and dynamically monitoring proliferation in real time without the use of chemical probes. The use of micro-electrodes to measure cellular impedance was pioneered by Giaever and Keese [29,30]. Since then, this technique has been applied to a number of biological studies that deal with cellular barrier function,

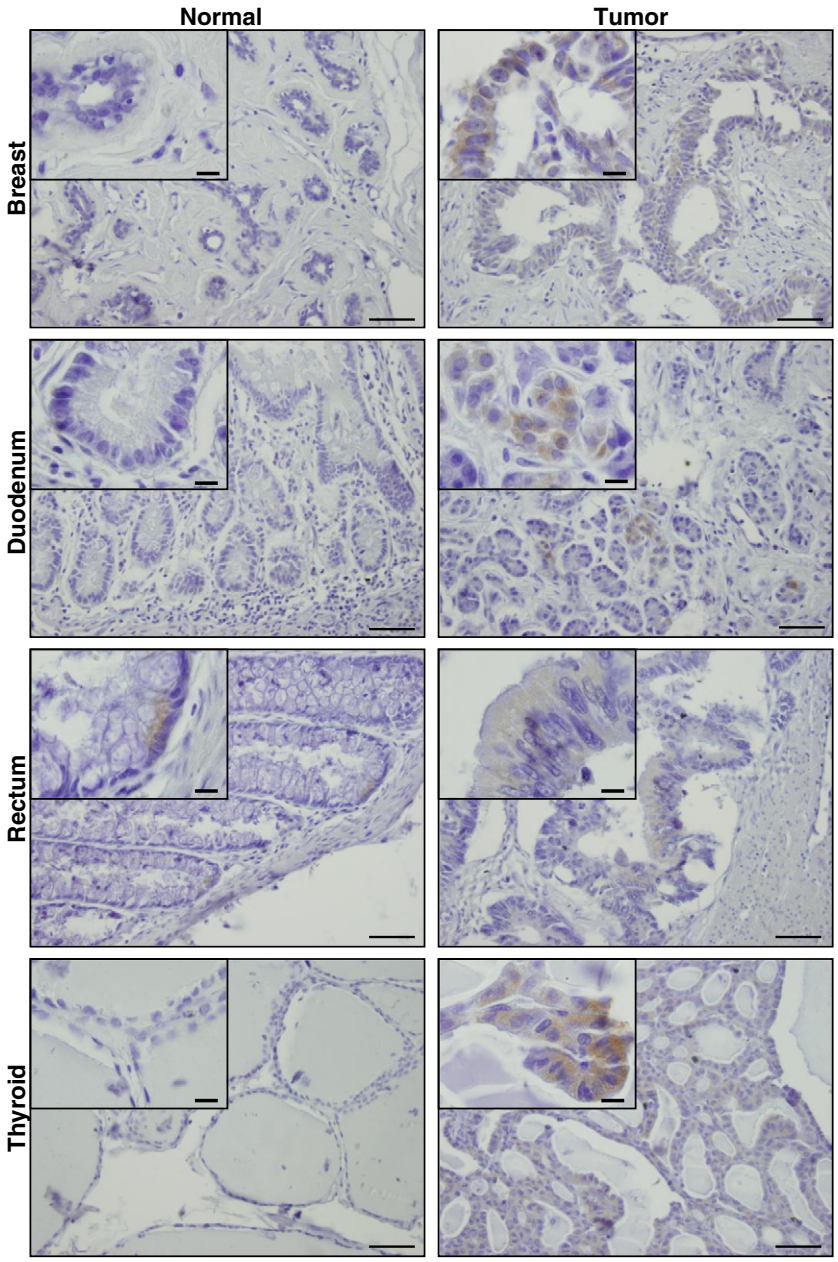

Fig. 4. Immunohistochemical staining of Nesprin-2 in human normal and tumor tissue array. Slides were stained with Nesprin-2 antibody, seen as brown coloring, and counterstained with Hematoxylin. Three independent observers note stain intensity for 47 normal tissues and 47 tumor tissues (Supplemental Table 1). Representative images from the tissues with the highest expression are shown. The large frames were taken with a 40× objective lens (50 μm scale bars), and the small frames in the upper left corners are at 100× (10 μm scale bars).

attachment, spreading, and adhesion [31–36]. In addition, frequency-dependent electrical impedance measurements have been used to evaluate the model parameters associated with cell–cell and cell–matrix junction formation [37–39]. In the present study, micro-impedance measurements were used to quantitatively examine proliferation and morphological changes such as cell–cell adhesion and cell–substrate adhesion under different concentrations of SS. Our data demonstrated the suppression of cell–cell adhesion and cell–substrate adhesion by SS in a dose-dependent manner. Subsequently, DICM was performed to observe cell morphology. Unlike phase contrast microscopy (PCM), DICM can visualize a wide variety of specimens such as very thin filaments, thick specimens, and sharp interfaces and can create realistic 3-dimensional shapes as an effective tool to qualitatively and quantitatively examine the effects of anti-tumorigenic compounds on cell adhesion. IRCM has been well known to provide a more comprehensive examination of cellular bottom morphology responses of when exposed to drugs. Early use of IRCM in cell biology goes back to Curtis' examination of how cells adhered to glass [40]. Subsequently, other groups improved this method by using a high numerical aperture objective lens, while a theoretical analysis attempted to quantify cell-substrate separation distances [41,42].

Microarrays were performed and two genes were identified as commonly down-regulated genes, based on biogenesis and cell organization pathways. The IDH2 and Nesprin-2 genes represent potential targets of SS since the IDH2 and Nesprin-2 mRNA seen in our microarray studies are confirmed by PCR. The fold reductions in these two genes observed through multiple replications of PCR correlates with the microarray data in that Nesprin-2 is more strongly down-regulated than IDH2 in both

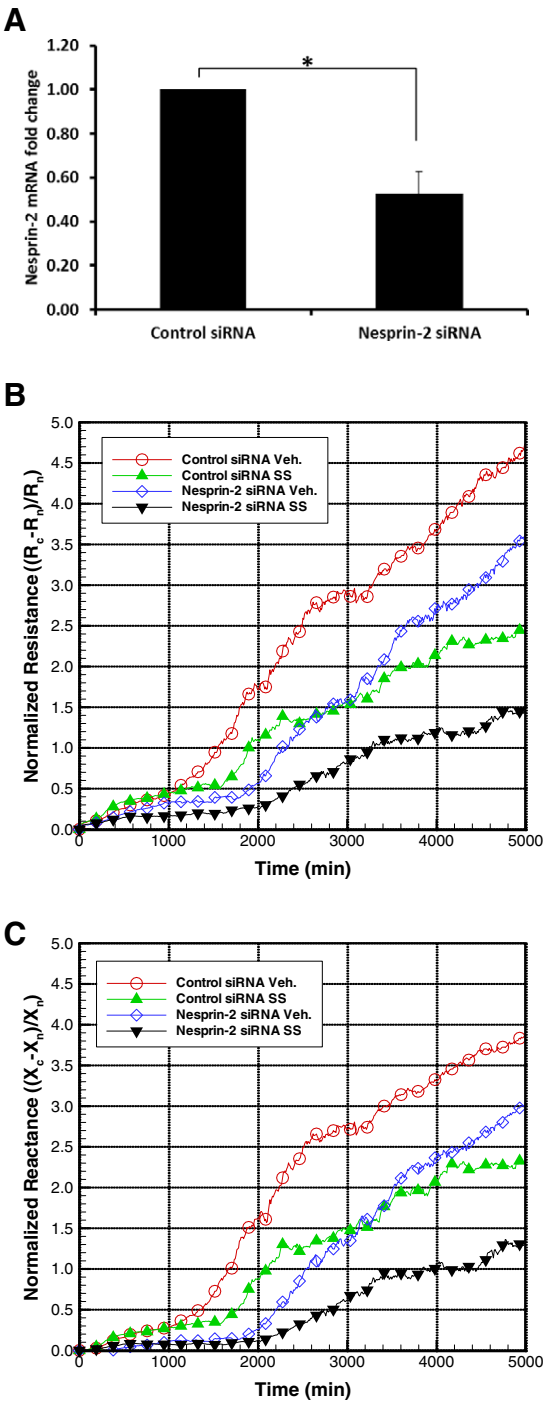

Fig. 5. The effect of Nesprin-2 mRNA knock-down of HCT-116 on micro-impedance. (A) Nesprin-2 expression knock-downed by siRNA. Nesprin-2 siRNA was transfected, and subsequently real time PCR was performed in triplicate to validate the siRNA in our system. GAPDH was used to amplify for RNA control. The graph shown represents a relative fold change, as the control siRNA set is 1.0 from three independent experiments. *P < 0.01. (B) Micro-impedance measurement of HCT-116 cells with knocked-down Nesprin-2 expression. HCT-116 cells were transfected with non-targeting control siRNA or siRNA Nesprin-2 and treated with vehicle or 30 μM SS. (C) The corresponding normalized reactance of these same cells was measured at the same time during this period. The terms *R* and *X* represent the resistance and reactance, respectively, and the subscripts *c* and *n* indicate cell covered and naked scans, respectively. Symbols represent 26 data intervals.

cases. Nesprin-2 was selected for this study based on its unique role as a link between the actin cytoskeleton and the nuclear envelope as well as its novelty as a potential oncogene. Interestingly, Nesprin-1 did not show any alterations in the presence of SS (Fig. 2A), indicating that NSAIDs affect Nesprin-2 in a specific manner.

While the NSAID doses used in this study were too high for serum relevancy, they were modest considering the obtainable concentrations in the colon. Sulindac is converted to the active metabolite SS in the liver and travels back to the gut through bile ducts where it is concentrated. Also, the natural colonic bacteria converts a large portion of sulindac to SS [43]. These two factors suggest that orally administered sulindac can lead to luminal SS concentrations in the colon that are higher concentration than obtainable in serum [44]. For example, animal studies have demonstrated that SS concentration in the colon mucosa is many-fold higher than serum levels [45]. The cells of the colonic epithelium could be subject to SS concentrations as high as 20-fold above what can be observed in the serum [44]. Based on the tissue to plasma level ratio of SS in the colon of 10–20 [44,45], other groups have justified using much higher SS concentrations, as high as 100–200 μM, as plausible in the human colon [46,47]. In addition, human familial adenomatous polyposis (FAP) patients can achieve 10–15 μM plasma concentrations of SS at doses that regress polyps [48,49]. Therefore, our doses used in this study could be in the range of clinical doses occurring in the intestine; however, our treatments were under serum free conditions which would differ substantially from physiological conditions.

Nesprin-2 has previously been reported to be present on the leading edge of migrating cells in wound-healing assays [18]. Due to this and its structural role, Nesprin-2 is an excellent candidate for investigation of the effects of SS on cell morphology and adhesion. Nesprin-2 mRNA expression is reduced by SS treatment in a time- and dose-dependent manner (Fig. 2). Other NSAIDs conventional as well as COX-1 and COX-2 specific all show reductions in Nesprin-2, with the most dramatic repression by SS. Interestingly, SS repression of Nesprin-2 is not limited to HCT-116 cells; however, this does not occur in all colorectal cancer cell lines tested. To examine mechanism by which SS suppresses Nesprin-2 expression, we investigated the transcriptional regulation of Nesprin-2. RNA stability appears to be involved in SS-induced Nesprin-2 down-regulation (Fig. 3E). Indeed, it has been reported that NSAID ibuprofen controls RNA stability of $p75^{NTR}$ in prostate cancer cells [50]. Another possible mechanism includes the β-catenin pathway. It has been reported that β-catenin participates in modulating cytoskeletal dynamics in association with the microfilament-bundling protein fascin [51]. SW480 cells did not show a significant reduction of Nesprin-2 in the presence of SS (Figs. 2B and 3D), explained by the cell context and probably by the strong β-catenin signaling in SW480 cells compared to others. Therefore, β-catenin signaling may inhibit SS-dependent Nesprin-2 down-regulation. However, further studies may be required to elucidate the molecular mechanism by which SS down-regulates Nesprin-2 in a cell-specific manner.

In the present study, siRNA consistently reduced Nesprin-2 mRNA expression by an average of 53%. This reduction in Nesprin-2 mRNA expression correlated nicely with the reduction in cell–cell adhesion and cell–substrate adhesion seen in the normalized resistance and cell's plasma membrane capacitance seen in the normalized reactance of the Nesprin-2 knockdown cells, as compared with the control siRNA-transfected cells treated with vehicle. In the case of the SS-treated cells, initial adhesion was similar at first for both Nesprin-2 knockdown and control siRNA cells. The Nesprin-2 knockdown cells showed reduced adhesion compared to the control siRNA cells. This suggests that reduction in Nesprin-2 by SS treatment could contribute to the loss of adhesion in colorectal cancer cells. In addition, we knocked-down Neprin-2 using shRNA which targets the CH2 domain (location of target shown in Fig. 2C) and measured micro-impedance (Supplementary Fig. 1). There was only a small reduction in Nesprin-2 mRNA, 23%, however, we still observed a significant loss of cell–cell/cell–substrate adhesion and a loss of membrane permeability as measured by micro-impedance.

Expression of Nesprin-2 in most tissues was too low to be routinely detected by immunohistochemistry using standard light microscopy, although the antibody used detects all isotypes. Notably increased staining for Nesprin-2 expression in tumor tissues over normal tissue can be seen in the mammary, duodenal, rectal, and thyroid tissues. Although

Nesprin-2 has been primarily detected in the nuclear membrane [18], our data suggest Nesprin-2 expression mostly in the cytoplasm of tumor tissue. This cytoplasmic localization in multiple neoplastic epithelial cells as well as the proliferative crypt cells of the rectum supports Nesprin-2's potential role as an oncogene. To the best of our knowledge, this is the first report that Nesprin-2 is more highly expressed in tumor tissues than in normal tissues.

5. Conclusions

The present study suggests that Nesprin-2 could be involved in oncogenesis and that SS treatment reduces its expression. This is strengthened by the increased Nesprin-2 expression observed in several different tumor types compared to normal tissue. This is further supported by Nesprin-2 knock-down cells mimicking the cell–cell adhesion and cell–substrate adhesion patterns seen with SS treatment proportional to the amount of suppression. Nesprin-2's vast size and position on the nuclear envelope and cytoplasm mark it as potential scaffolding for many other protein–protein interactions. Further study of Nesprin-2 could lead to a novel target for cancer treatment.

Supplementary data to this article can be found online at http://dx.doi.org/10.1016/j.bbagen.2013.09.032.

Conflict of interest statement

No conflict of interest exists in the submission of this manuscript.

Acknowledgements

The authors thank Dr. Maria Cekanova for her technical assistance and Misty Bailey for her critical review.

References

[1] A. Reddy, W.G. Kaelin Jr., Using cancer genetics to guide the selection of anticancer drug targets, Curr. Opin. Pharmacol. 2 (2002) 366–373.
[2] P. Ricchi, S. Pignata, R.V. Iaffaioli, B. Daniele, Cyclo-oxygenase inhibition in colorectal adenomas and cancer, J. Clin. Gastroenterol. 37 (2003) 281–287.
[3] M.M. Taketo, Cyclooxygenase-2 inhibitors in tumorigenesis (part I), J. Natl. Cancer Inst. 90 (1998) 1529–1536.
[4] J.A. Baron, Aspirin and NSAIDs for the prevention of colorectal cancer, Recent Results Cancer Res. 181 (2009) 223–229.
[5] T. Iwama, NSAIDs and colorectal cancer prevention, J. Gastroenterol. 44 (Suppl. 19) (2009) 72–76.
[6] G.A. Piazza, A.K. Rahm, T.S. Finn, B.H. Fryer, H. Li, A.L. Stoumen, R. Pamukcu, D.J. Ahnen, Apoptosis primarily accounts for the growth-inhibitory properties of sulindac metabolites and involves a mechanism that is independent of cyclooxygenase inhibition, cell cycle arrest, and p53 induction, Cancer Res. 57 (1997) 2452–2459.
[7] C.H. Chiu, M.F. McEntee, J. Whelan, Sulindac causes rapid regression of preexisting tumors in Min/+ mice independent of prostaglandin biosynthesis, Cancer Res. 57 (1997) 4267–4273.
[8] X. Wang, P.J. Kingsley, L.J. Marnett, T.E. Eling, The role of NAG-1/GDF15 in the inhibition of intestinal polyps in APC/Min mice by sulindac, Cancer Prev. Res. (Phila.) 4 (2011) 150–160.
[9] P.L. Rice, J. Kelloff, H. Sullivan, L.J. Driggers, K.S. Beard, S. Kuwada, G. Piazza, D.J. Ahnen, Sulindac metabolites induce caspase- and proteasome-dependent degradation of beta-catenin protein in human colon cancer cells, Mol. Cancer Ther. 2 (2003) 885–892.
[10] S.J. Baek, K.S. Kim, J.B. Nixon, L.C. Wilson, T.E. Eling, Cyclooxygenase inhibitors regulate the expression of a TGF-beta superfamily member that has proapoptotic and antitumorigenic activities, Mol. Pharmacol. 59 (2001) 901–908.
[11] S.J. Baek, L.C. Wilson, T.E. Eling, Resveratrol enhances the expression of non-steroidal anti-inflammatory drug-activated gene (NAG-1) by increasing the expression of p53, Carcinogenesis 23 (2002) 425–432.
[12] S.J. Shiff, M.I. Koutsos, L. Qiao, B. Rigas, Nonsteroidal antiinflammatory drugs inhibit the proliferation of colon adenocarcinoma cells: effects on cell cycle and apoptosis, Exp. Cell Res. 222 (1996) 179–188.
[13] Y. Goldberg, I.I. Nassif, A. Pittas, L.L. Tsai, B.D. Dynlacht, B. Rigas, S.J. Shiff, The anti-proliferative effect of sulindac and sulindac sulfide on HT-29 colon cancer cells: alterations in tumor suppressor and cell cycle-regulatory proteins, Oncogene 12 (1996) 893–901.
[14] I. Casanova, M. Parreno, L. Farre, S. Guerrero, M.V. Cespedes, M.A. Pavon, F.J. Sancho, E. Marcuello, M. Trias, R. Mangues, Celecoxib induces anoikis in human colon carcinoma cells associated with the deregulation of focal adhesions and nuclear translocation of p130Cas, Int. J. Cancer 118 (2006) 2381–2389.
[15] M.J. Weyant, A.M. Carothers, M.E. Bertagnolli, M.M. Bertagnolli, Colon cancer chemopreventive drugs modulate integrin-mediated signaling pathways, Clin. Cancer Res. 3 (2000) 949–956.
[16] N.N. Mahmoud, R.T. Bilinski, M.R. Churchill, W. Edelmann, R. Kucherlapati, M.M. Bertagnolli, Genotype-phenotype correlation in murine Apc mutation: differences in enterocyte migration and response to sulindac, Cancer Res. 59 (1999) 353–359.
[17] N.N. Mahmoud, S.K. Boolbol, R.T. Bilinski, C. Martucci, A. Chadburn, M.M. Bertagnolli, Apc gene mutation is associated with a dominant-negative effect upon intestinal cell migration, Cancer Res. 57 (1997) 5045–5050.
[18] Y.Y. Zhen, T. Libotte, M. Munck, A.A. Noegel, E. Korenbaum, NUANCE, a giant protein connecting the nucleus and actin cytoskeleton, J. Cell Sci. 115 (2002) 3207–3222.
[19] V.C. Padmakumar, S. Abraham, S. Braune, A.A. Noegel, B. Tunggal, I. Karakesisoglou, E. Korenbaum, Enaptin, a giant actin-binding protein, is an element of the nuclear membrane and the actin cytoskeleton, Exp. Cell Res. 295 (2004) 330–339.
[20] D.T. Warren, Q. Zhang, P.L. Weissberg, C.M. Shanahan, Nesprins: intracellular scaffolds that maintain cell architecture and coordinate cell function? Expert Rev. Mol. Med. 7 (2005) 1–15.
[21] Q. Zhang, C.D. Ragnauth, J.N. Skepper, N.F. Worth, D.T. Warren, R.G. Roberts, P.L. Weissberg, J.A. Ellis, C.M. Shanahan, Nesprin-2 is a multi-isomeric protein that binds lamin and emerin at the nuclear envelope and forms a subcellular network in skeletal muscle, J. Cell Sci. 118 (2005) 673–687.
[22] W. Lu, M. Schneider, S. Neumann, V.M. Jaeger, S. Taranum, M. Munck, S. Cartwright, C. Richardson, J. Carthew, K. Noh, M. Goldberg, A.A. Noegel, I. Karakesisoglou, Nesprin interchain associations control nuclear size, Cell. Mol. Life Sci. 69 (2012) 3493–3509.
[23] R.N. Rashmi, B. Eckes, G. Glockner, M. Groth, S. Neumann, J. Gloy, L. Sellin, G. Walz, M. Schneider, I. Karakesisoglou, L. Eichinger, A.A. Noegel, The nuclear envelope protein Nesprin-2 has roles in cell proliferation and differentiation during wound healing, Nucleus (Austin, Tex.) 3 (2012) 172–186.
[24] T. Libotte, H. Zaim, S. Abraham, V.C. Padmakumar, M. Schneider, W. Lu, M. Munck, C. Hutchison, M. Wehnert, B. Fahrenkrog, U. Sauder, U. Aebi, A.A. Noegel, I. Karakesisoglou, Lamin A/C-dependent localization of Nesprin-2, a giant scaffolder at the nuclear envelope, Mol. Biol. Cell 7 (2005) 3411–3424.
[25] D. Rajgor, J.A. Mellad, F. Autore, Q. Zhang, C.M. Shanahan, Multiple novel Nesprin-1 and Nesprin-2 variants act as versatile tissue-specific intracellular scaffolds, PloS ONE 7 (2012) e40098.
[26] S. Arndt, J. Seebach, K. Psathaki, H.J. Galla, J. Wegener, Bioelectrical impedance assay to monitor changes in cell shape during apoptosis, Biosens. Bioelectron. 19 (2004) 583–594.
[27] H. Yin, Frank Lei Wang, Angelo Lei Wang, Jing Cheng, Yuxiang Zhou, Bioelectrical impedance assay to monitor changes in aspirin-treated human colon cancer HT-29 cell shape during apoptosis, Anal. Lett. 40 (2007) 85–94.
[28] S.J. Baek, T.E. Eling, Changes in gene expression contribute to cancer prevention by COX inhibitors, Prog. Lipid Res. 45 (2006) 1–16.
[29] I. Giaever, C.R. Keese, Monitoring fibroblast behavior in tissue culture with an applied electric field, Proc. Natl. Acad. Sci. U. S. A. 81 (1984) 3761–3764.
[30] I. Giaever, C.R. Keese, Use of electric fields to monitor the dynamical aspect of cell behavior in tissue culture, IEEE Trans. Biomed. Eng. BME-33 (1986) 242–247.
[31] A.R. Burns, R.A. Bowden, S.D. MacDonell, D.C. Walker, T.O. Odebunmi, E.M. Donnachie, S.I. Simon, M.L. Entman, C.W. Smith, Analysis of tight junctions during neutrophil transendothelial migration, J. Cell Sci. 113 (2000) 45–57.
[32] J.P. Gainor, C.A. Morton, J.T. Roberts, P.A. Vincent, F.L. Minnear, Platelet-conditioned medium increases endothelial electrical resistance independently of cAMP/PKA and cGMP/PKG, Am. J. Physiol. Heart Circ. Physiol. 281 (2001) H1992–H2001.
[33] N. Kataoka, K. Iwaki, K. Hashimoto, S. Mochizuki, Y. Ogasawara, M. Sato, K. Tsujioka, F. Kajiya, Measurements of endothelial cell-to-cell and cell-to-substrate gaps and micromechanical properties of endothelial cells during monocyte adhesion, Proc. Natl. Acad. Sci. 99 (2002) 15638–15643.
[34] C.K. Choi, A.E. English, S.I. Jun, K.D. Kihm, P.D. Rack, An endothelial cell compatible biosensor fabricated using optically thin indium tin oxide silicon nitride electrodes, Biosens. Bioelectron. 22 (2007) 2585–2590.
[35] C.K. Choi, C.H. Margraves, A.E. English, K.D. Kihm, Multicontrast microscopy technique to dynamically fingerprint live-cell focal contacts during exposure and replacement of a cytotoxic medium, J. Biomed. Opt. 13 (2008) 054069.
[36] C.K. Choi, A.E. English, K.D. Kihm, C.H. Margraves, Simultaneous dynamic optical and electrical properties of endothelial cell attachment on indium tin oxide bioelectrodes, J. Biomed. Opt. 12 (2007) 064028.
[37] I. Giaever, C.R. Keese, Micromotion of mammalian cells measured electrically, Proc. Natl. Acad. Sci. U. S. A. 88 (1991) 7896–7900.
[38] I. Giaever, C.R. Keese, Correction: micromotion of mammalian cells measured electrically, Proc. Natl. Acad. Sci. U. S. A. 90 (1993) 1634.
[39] A.E. English, C.P. Plaut, A.B. Moy, A Riemannian manifold analysis of endothelial cell monolayer impedance parameter precision, J. Math. Biol. 55 (2007) 721–743.
[40] A.S. Curtis, The mechanism of adhesion of cells to glass. A study by interference reflection microscopy, J. Cell Biol. 20 (1964) 199–215.
[41] D. Gingell, I. Todd, Interference reflection microscopy. A quantitative theory for image interpretation and its application to cell-substratum separation measurement, Biophys. J. 26 (1979) 507–526.
[42] C.S. Izzard, L.R. Lochner, Cell-to-substrate contacts in living fibroblasts: an interference reflexion study with an evaluation of the technique, J. Cell Sci. 21 (1976) 129–159.
[43] H. Strong, N. Warner, A. Renwick, C. George, Sulindac metabolism: the importance of an intact colon, Clin. Pharmacol. Ther. 38 (1985) 387–393.

[44] W.R. Waddell, G.F. Ganser, E.J. Cerise, R.W. Loughry, Sulindac for polyposis of the colon, Am. J. Surg. 157 (1989) 175–179.
[45] D. Duggan, K. Hooke, S. Hwang, Kinetics of the tissue distributions of sulindac and metabolites. Relevance to sites and rates of bioactivation, Drug Metab. Dispos. 8 (1980) 241–246.
[46] R. Hanif, A. Pittas, Y. Feng, M.I. Koutsos, L. Qiao, L. Staiano-Coico, S.I. Shiff, B. Rigas, Effects of nonsteroidal anti-inflammatory drugs on proliferation and on induction of apoptosis in colon cancer cells by a prostaglandin-independent pathway, Biochem. Pharmacol. 52 (1996) 237–245.
[47] D.P. Kunte, R.K. Wali, J.L. Koetsier, H.K. Roy, Antiproliferative effect of sulindac in colonic neoplasia prevention: role of COOH-terminal Src kinase, Mol. Cancer Ther. 7 (2008) 1797–1806.
[48] B.N. Swanson, V.K. Boppana, P.H. Vlasses, G.I. Holmes, K. Monsell, R.K. Ferguson, Sulindac disposition when given once and twice daily, Clin. Pharmacol. Ther. 32 (1982) 397–403.
[49] D. Duggan, L. Hare, C. Ditzler, B. Lei, K. Kwan, The disposition of sulindac, Clin. Pharmacol. Ther. 21 (1977) 326.
[50] E.J. Quann, F. Khwaja, K.H. Zavitz, D. Djakiew, The aryl propionic acid R-flurbiprofen selectively induces p75NTR-dependent decreased survival of prostate tumor cells, Cancer Res. 67 (2007) 3254–3262.
[51] Y.S. Tao, R.A. Edwards, B. Tubb, S. Wang, J. Bryan, P.D. McCrea, Beta-catenin associates with the actin-bundling protein fascin in a noncadherin complex, J. Cell Biol. 134 (1996) 1271–1281.